Geochemical Perspectives Letters

Pyrite-based trace element fingerprints for methane and oil seepage

D. Smrzka, Z. Lin, P. Monien, T. Chen, W. Bach, J. Peckmann, G. Bohrmann

Supplementary Information

The Supplementary Information includes:

- Methods
- Results
- Tables S-1 to S-4
- Figures S-1 to S-3

Methods

This supplementary information includes details on pyrite sampling, sample preparation and geochemical analyses. Pyrite was sampled from oil seep sediments at Mictlan Knoll, Tsanyao Yang Knoll and Knoll 2000 (Campeche Knolls, Sahling *et al.,* 2016), as well as from Challenger Knoll (Sigsbee Knolls; Fig. 1a; Sahling and Bohrmann, 2017). Methane seepage-derived pyrite was sampled from cores taken at Four-Way-Closure Ridge (FWCR) offshore Taiwan (Fig. 1b; Tseng *et al*., 2023). The cores were sampled in intervals of 20 cm, each sample containing ca. 30 grams of sediment. Sediment samples were freeze-dried over 24 h, and subsequently powdered by hand using an agate pestle and mortar. The ground sediments were then sieved with deionised water through a 0.063 mm sieve, and pyrite aggregates were hand-picked under a binocular microscope from the coarse fraction. Pyrite grains were mounted onto epoxy discs, polished to a smooth surface and coated with carbon for electron microprobe analysis (EMPA). Scanning electron microscopy (SEM) was conducted using a Zeiss Supra 40 instrument equipped with a Bruker EDX system. All pyrite samples are present as tubular aggregates, which are themselves composed of smaller framboidal clusters and aggregates of pyrite crystals (Fig. S-1). Uncoated discs were used for laser ablation inductively coupled plasma mass spectrometry (LA-ICP-MS). Prior to EMPA and LA-ICP-MS, mounted pyrite was investigated by reflected light microscopy to select suitable samples for further analyses.

Major element composition of pyrite was determined using a Cameca SX-100 electron microprobe at the Faculty of Geosciences, University of Bremen. Analytical conditions included an acceleration voltage of 20 kV, beam current of 20 nA, and a defocussed beam between 1 and 10 µm diameter. Counting times were 20 s on peak and 10 s on background. For quantification natural minerals from the faculty collection and from the Smithsonian Institution (Jarosewich *et al*., 1980), and the built-in PAP matrix correction were used. Spot sizes and locations were chosen in order to account for sample heterogeneity for each sample in order to arrive at a representative average Fe value used for subsequent LA-ICP-MS data quantification.

LA-ICP-MS was conducted using a NewWave UP 193 nm solid-state laser coupled to a Thermo-Finnigan Element 2 HR-ICP-MS at the University of Bremen. The ICP-MS was operated with a plasma power of 1200 W, while helium (He; 0.8 L min-1) was used as a sample gas, and argon (Ar; 0.8 L min^{-1}) was used as carrier gas. A single spot ablation pattern with a laser pulse rate of 5 Hz, an irradiance of approx. 1.3 GW cm^{-2}, and beam diameters of 30 µm were applied. Total analysis time for each spot was 60 s, including 30 s for gas blank analysis. Pre-ablation was conducted with a beam diameter slightly larger than the beam diameter used for the actual measurement. After every 5 to 10 samples NIST610 glass was analysed as external calibration standard using the values of Jochum *et al*. (2011). During laser ablation each sample point was monitored using the time-resolved chromatograms during the measurements in order to discard any sample with irregular or low iron content. The Cetac GeoPro™ software was used for data quantification and ^{56}Fe was used as the internal standard. The NIST610 (USGS) glass standard was used for external calibration for Mn, Zn, Mo, Cd, U and Cu. Due to the lack of sufficient sulfide reference material, data quality was assessed by regular analyses of USGS reference materials BCR-2G, BHVO-2G (basaltic glasses) and MASS-1 sulfide standard (USGS, Wilson *et al*., 2002) along with the samples. Because these glass reference materials are unsuitable for the quantitative analysis of sulfides, a matrix normalisation calibration strategy was applied (Liu *et al*., 2008; Yuan *et al*., 2012). Trace elements in pyrite were analysed by multi-external standards with matrix normalisation and an iron internal standardisation. This calibration method employed a basaltic glass reference material (BHVO-2G) as a transition bridge and multi-glass reference materials with matrix normalisation plus internal standardisation (Fe as the internal standard) to determine the trace elemental composition of sulfide minerals (cf. Yuan *et al*., 2012; Miao *et al*., 2022). The MASS-1 reference material was used as a secondary independent control standard given that the silicate glass reference materials are not well suited for analysis if used alone. The analytical results of trace elements obtained by multi-external standards with matrix normalisation plus Fe internal standardisation show relative standard deviations (RSD) below 10 % except for Zn, as well as relative errors better than 10 % for all measured elements except for Mo and Zn (Table S-2).

Trace element composition of bulk sediments was conducted using an Agilent Technologies 7700x quadrupole ICP-MS at Nanjing FocuMS Technology Co. Ltd. About 40 mg powder was transferred into high-pressure PTFE bombs mixed with 0.5 ml 60 wt. % HNO_3 and 1.0 ml 40 % HF. These bombs were sealed and placed in the oven at 195 ℃ for 72 hours to ensure complete digestion. After cooling, the bombs were opened, dried down on a hotplate, treated with 5 ml 15 wt. % HNO_3 and 1ml Rh internal standard, then sealed and placed in the oven at 150 ℃ overnight. Then Aliquot of the digestions were diluted 2000-fold and nebulised into ICP-MS to determine trace elements. Geochemical reference materials of basalt (BHVO-2) and andesite (AGV-2) were used as quality control. Deviation was better than 10 % for all measured elements.

Results

There is no evidence for hydrothermalism in both study areas (MacDonald *et al*., 2004; Sahling *et al*., 2016; Tseng *et al*., 2023), and can therefore be ruled out as a potential source for trace element enrichment to the sediments and pyrites. Trace element geochemistry shows that Mn/Fe *vs.* Mo distributions in pyrite and bulk sediments show similar distribution patterns (Fig. S-2a). Zinc is enriched in methane seep sediments, whereas Cu is enriched in oil seep sediments (Fig. S-2b). Also, Ni is more significantly enriched in these latter sediments than in pyrite (Fig. S-2c). The content of detrital elements Al and Ti in sediments from the South China Sea sites is, on average, higher than in the Gulf of Mexico oil seep sediments (Fig. S-2d-f). Further, there is no correlation between Mn and Al in the sediments (Fig. S-2d), suggesting that Mn is not derived from detrital alumosilicate material.

This suggests the following:

1. Alumosilicates are not responsible for Mn, Mo, Zn, Cu, Ni, and V enrichments in pyrite. Moreover, Mn shows no correlation to Al in the sediment, indicating that its enrichment is authigenic.
2. Manganese and Mo enrichment at oil seeps is authigenic, in the pyrite and the sediments, being most likely associated with the presence and oxidation of oil in the sediments as outlined in in the discussion chapter “A combined Fe-Mn-Mo fingerprint” in the main article.

3. Copper and Zn show different patterns in the sediment, suggesting that these elements are enriched by an authigenic process in pyrite as outlined in the discussion chapter "A combined Cu-Zn-Ni-V fingerprint" (main article)., and that they have high affinities for pyrite incorporation.
4. Nickel is enriched in oil seep sediments, probably due to the presence of oil and the high Ni content of oils (cf. Smrzka *et al*., 2019).

We have added a bar plot (Fig. S-3) showing calculated enrichment factors (EFs) of the host sediments (EF = (EL/Alsample)/(EL/Alshale)).

Supplementary Tables

Tables S-1 to S-4 are available for download (Excel) from the online version of this article at https://doi.org/10.7185/geochemlet.2409

Table S-1 Major and trace elemental composition of pyrite derived from oil- and methane-dominated seeps, all values in ppm. All data acquired by LA-ICP-MS except for Fe, which was determined via EMPA.

Table S-2 Precision and accuracy of determined major and trace elements in pyrite shown in Table S-1.

Table S-3 Trace element geochemistry of sediment cores.

Table S-4 Calculated sediment trace element enrichment factors.

Supplementary Figures

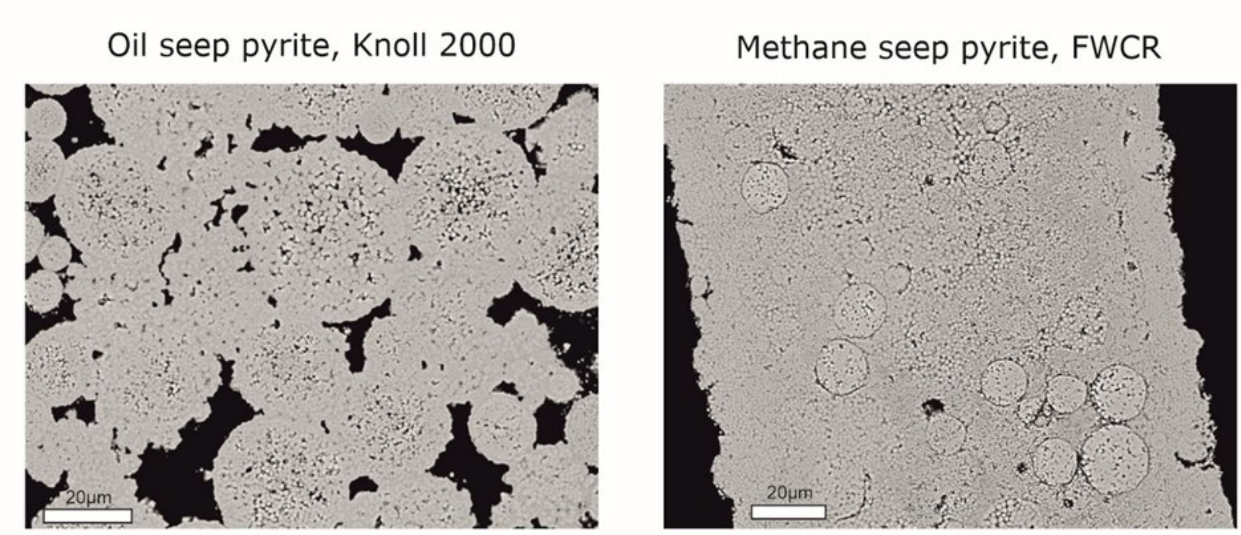

Figure S-1 SEM images of authigenic pyrite from oil and methane seep sediments.

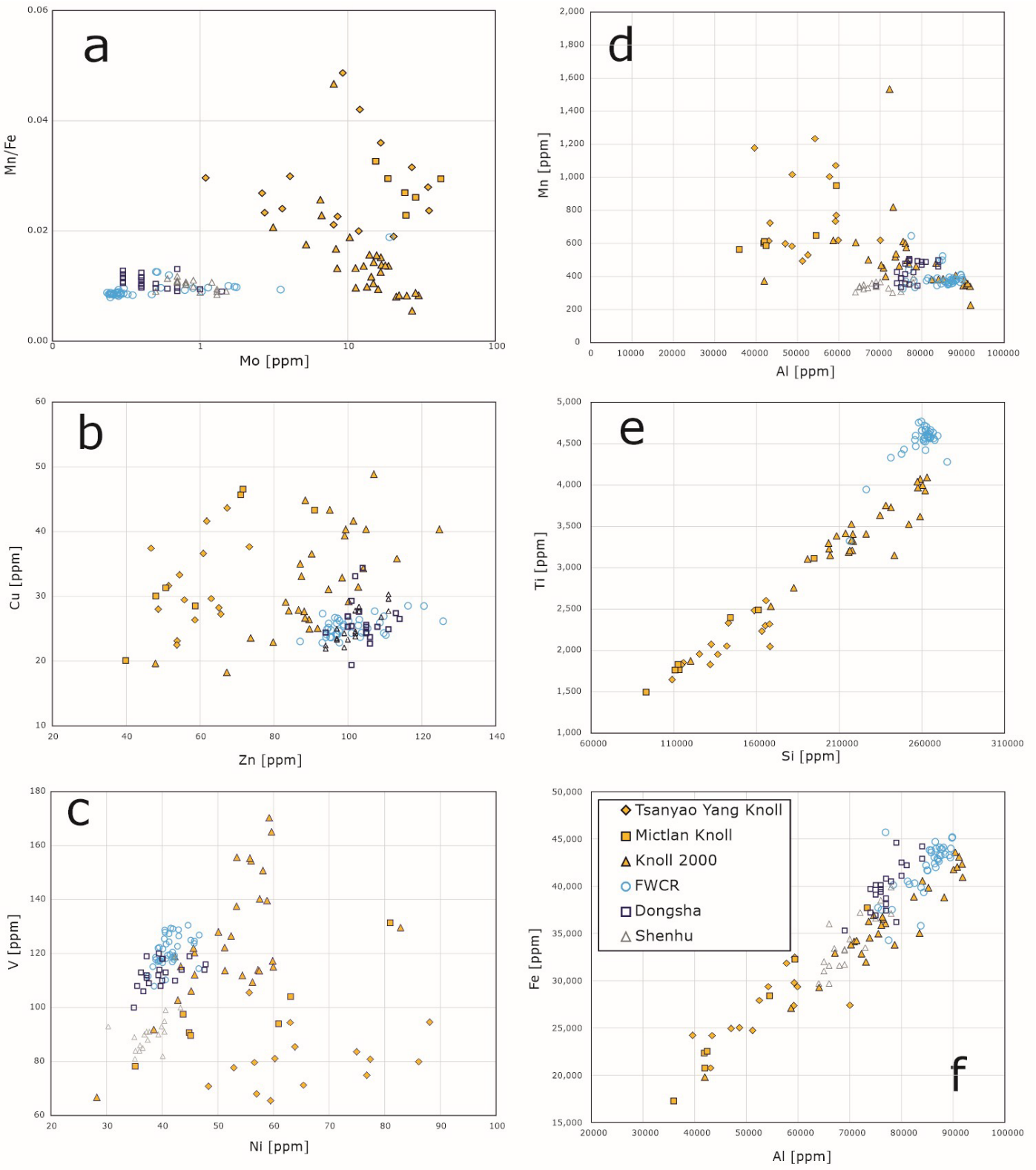

Figure S-2 Trace element distribution in oil- and methane-seep sediments.

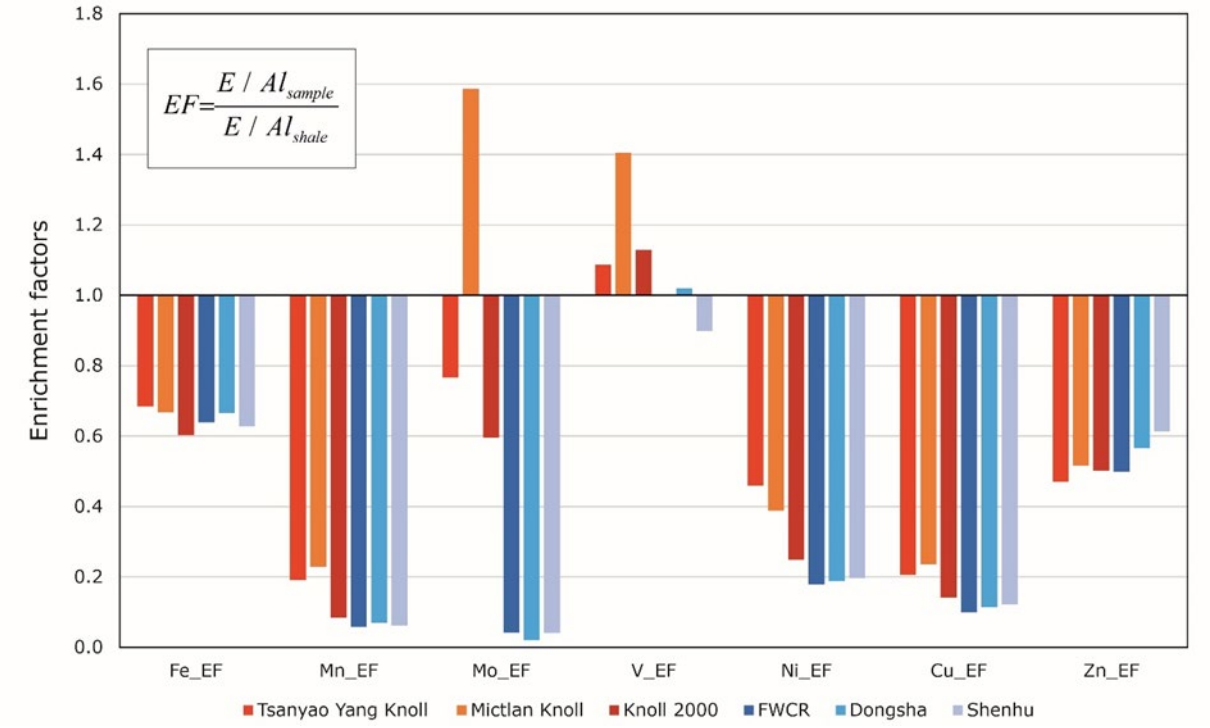

Figure S-3 Calculated trace element enrichment factors (EFs) in oil- and methane-seep sediments.

Supplementary Information References

Jarosewich, E., Nelen, J.A., Norberg, J.A. (1980) Reference samples for electron microprobe analysis. *Geostandards Newsletter* 4, 43-47. https://doi.org/10.1111/j.1751-908X.1980.tb00273.x.

Jochum, K.P., Weis, U., Stoll, B., Kuzmin, D., Yang, Q., Raczek, I., Jacob, D.E., Stracke, A., Birbaum, K., Frick, D.A., Günther, D., Enzweiler, J. (2011) Determination of reference values for NIST SRM 610-617 glasses following ISO guidelines. *Geostandards and Geoanalytical Research* 35, 397-429. https://doi.org/10.1111/j.1751-908X.2011.00120.x.

Liu, Y., Hu, Y., Gao, S., Günther, D., Xu, J., Gao, C., Chen, H. (2008) *In situ* analysis of major and trace elements of anhydrous minerals by LA-ICP-MS without applying an internal standard. *Chemical Geology* 257, 34-43. https://doi.org/10.1016/j.chemgeo.2008.08.004.

MacDonald, I.R., Bohrmann, G., Escobar, E., Abegg, F., Blanchon, P., Blinova, V., Brückmann, W., Drews, M., Eisenhauer, A., Han, X., Heeschen, K., Meier, F., Mortera, C., Naehr, T., Orcutt, B., Bernard, B., Brooks, J., De Faragó, M. (2004) Asphalt Volcanism and Chemosynthetic Life in the Campeche Knolls, Gulf of Mexico. *Science* 304, 999-1002. https://doi.org/10.1126/science.1097154.

Miao, X., Feng, X., Li, J., Liu, X., Liang, J., Feng, J., Xiao, Q., Dan, X., Wie, J. (2022) Enrichment mechanism of trace elements in pyrite under methane seepage. *Geochemical Perspectives Letters* 21, 18-22. https://doi.org/10.7185/geochemlet.2211.

Sahling, H., Bohrmann, G., Cruise Participants (2017) R/V METEOR Cruise Report M114, Natural hydrocarbon seepage in the southern Gulf of Mexico, Kingston - Kingston, 12 February - 28 March 2015. Berichte, MARUM–Zentrum für Marine Umweltwissenschaften, Fachbereich Geowissenschaften, Universität Bremen 315, 1–214. urn:nbn:de:gbv:46-00105897-18.

Sahling, H., Borowski, C., Escobar-Briones, E., Gaytán-Caballero, A., Hsu, C.-W., Loher, M., MacDonald, I., Marcon, Y., Pape, T., Römer, M., Rubin-Blum, M., Schubotz, F., Smrzka, D., Wegener, G., Bohrmann, G. (2016) Massive asphalt deposits, oil seepage, and gas venting support abundant chemosynthetic communities at the Campeche Knolls, southern Gulf of Mexico. *Biogeosciences* 13, 4491-4512. https://doi.org/10.5194/bg-13-4491-2016.

Tseng, Y., Römer, M., Lin, S., Pape, T., Berndt, C., Chen, T.-T., Paull, C.K., Caress, D.W., Bohrmann, G. (2023) Yam Seep at Four-Way Closure Ridge: a prominent active gas seep system at the accretionary wedge SW offshore Taiwan. *International Journal of Earth Sciences* 112, 1043-1061. https://doi.org/10.1007/s00531-022-02280-4.

Wilson, S.A., Ridley, W.I., Koenig, A.E. (2002) Development of sulfide calibration standards for the laser ablation inductively-coupled plasma mass spectrometry technique. *Journal of Analytical Atomic Spectrometry* 17, 406-409. https://doi.org/10.1039/B108787H.

Yuan, J.-H., Zhan, X.-C., Fan, C.-Z., Zhao, L.-H., Sun, D.-Y., Jia, Z.-R., Hu, M.-Y., Kuai, L.-J. (2012) Quantitative analysis of sulfide minerals by laser ablation-inductively coupled plasma-mass spectrometry using glass reference materials with matrix normalization plus sulfur internal standardization calibration. *Chinese Journal of Analytical Chemistry* 40, 201-207. https://doi.org/10.1016/S1872-2040(11)60528-8.